European Journal of Medicinal Chemistry 276 (2024) 116697

Contents lists available at ScienceDirect

European Journal of Medicinal Chemistry

journal homepage: www.elsevier.com/locate/ejmech

Research paper

Anticancer activity of new water-soluble sulfonated thiosemicarbazone copper(II) complexes targeting disulfide isomerase

Francesca Miglioli [a], Michele De Franco [b], Jennifer Bartoli [a], Mirco Scaccaglia [a], Giorgio Pelosi [a], Cristina Marzano [b], Dominga Rogolino [a], Valentina Gandin [b,**,1], Mauro Carcelli [a,*,1]

[a] Department of Chemistry, Life Sciences, Environmental Sustainability, University of Parma, Parco Area Delle Scienze 11/A, 43124, Parma, Italy
[b] Department of Pharmaceutical and Pharmacological Sciences, University of Padova, Via F. Marzolo 5, 35131, Padova, Italy

ARTICLE INFO

Keywords:
Thiosemicarbazones
Copper complexes
Anticancer activity
Protein disulfide isomerase
Water soluble metal complexes
Cuproptosis
X-ray structure
Coordination compounds

ABSTRACT

Copper complexes have shown promising anticancer properties, but they are often poorly soluble in aqueous solutions, thus limiting their possible medical developments and applications. We have recently isolated some copper(II) complexes with salicylaldehyde thiosemicarbazone ligands exhibiting remarkable nanomolar cytotoxic activity, but *in vivo* tests evidenced several difficulties related to their poor solubility. To overcome these limitations and increase solubility in aqueous solution, herein we report the synthetic strategy that led to the introduction of the sulfonic group on the ligands, then separated as salts (**NaH_2L^1** - **NaH_2L^5**), as well as the synthesis and characterization of the related copper(II) complexes. The characterization of the complexes is completed by the analysis of the structures obtained by X-rays diffraction on single crystals on the species $[Cu(HL^5)(H_2O)]_2 2H_2O$, $[Cu(HL^2)(H_2O)_2]\cdot 2H_2O$, and $[Cu(HL^1)(H_2O]_2 2H_2O$. While the uncoordinated ligands do not affect cancer cell viability, copper(II) complexes exhibit low to sub-micromolar cytotoxic activity, which is maintained in 3D (HCT-15 and 2008) spheroidal models of cancer cell. Notably, copper(II) complexes were selective towards cancer cells, showing high selectivity indexes. Investigations focused on elucidating the mechanism of action evidenced the protein disulfide-isomerase as an innovative molecular target for this class of water-soluble copper(II) complexes. Finally, preliminary *in vivo* experiments performed with the most representative derivative in the murine Lewis Lung Carcinoma, highlight its significant antitumor efficacy and better tolerability profile with respect to the reference metallodrug, suggesting for this sulfonated Cu(II) complex a potential clinical relevance.

1. Introduction

Thiosemicarbazones (TSCs) represent a versatile class of ligands endowed with a broad spectrum of biological activities, including antiviral, antibacterial and anticancer properties [1,2]. To date, Triapine (3-AP, Fig. 1) has entered several clinical trials [3,4], and other promising TSCs (di-2-pyridylketone 4-cyclohexyl-4-methyl-3-thiosemicarbazone, DpC; (*E*)-N′-(6,7-dihydroquinolin-8(5H)-ylidene)-4-(pyridin-2-yl) piperazine-1-carbothiohydrazide, COTI-2; Fig. 1) have recently joined the Triapine in the anticancer arena [5,6]. TSCs have excellent chelating properties towards a wide range of biologically relevant metal ions and coordination might result in enhanced anticancer potency versus the free ligand [7,8]. It is noteworthy that these ligands can be easily functionalized to tune important features of the corresponding metal complexes, such as lipophilicity, solubility and stability towards biological competitors, leading to favorable pharmacological profiles. Moreover, the combination of TSCs and metal ions, according to structural functionalizations and coordinating modalities, can lead to diversified biological pathways, activating alternative modes of action respect to the free ligand [9–11]. Many different targets have been identified for diverse TSCs metal complexes: they can inhibit enzymes involved in DNA synthesis and polymerization [12,13], sequestrate intracellular iron and induce the overproduction of reactive oxygen species (ROS) [14,15], or they can alter copper(II) homeostasis [16,17]. To this regard, copper and its coordination compounds have been receiving increasing attention, since they could provide the opportunity

* Corresponding author.
** Corresponding author.
E-mail addresses: valentina.gandin@unipd.it (V. Gandin), mauro.carcelli@unipr.it (M. Carcelli).
[1] Corresponding authors contributed equally to the work.

https://doi.org/10.1016/j.ejmech.2024.116697
Received 30 April 2024; Received in revised form 26 June 2024; Accepted 17 July 2024
Available online 18 July 2024
0223-5234/© 2024 The Authors. Published by Elsevier Masson SAS. This is an open access article under the CC BY-NC-ND license (http://creativecommons.org/licenses/by-nc-nd/4.0/).

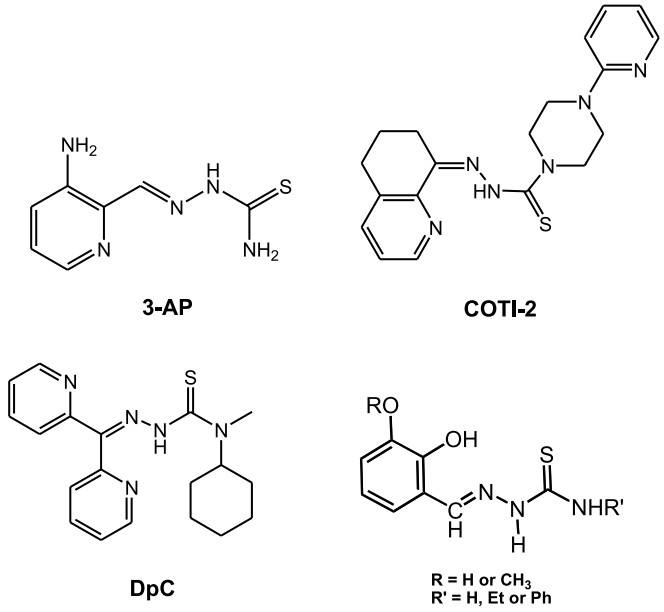

Fig. 1. Schematic representation of some TSCs in clinical trial (3-AP, COTI-2, DpC) and of the salicylaldehyde thiosemicarbazone derivatives previously studied [24].

to develop alternatives to other metal-based drugs used in clinical practice [18]. In fact, even if *cis*-platin and its derivatives represent a milestone in the fight against cancer, poor selectivity, important side effects and resistance phenomena limit their efficacy [19]. Looking for improved selectivity versus platinum-based drugs, the crucial role of endogenous copper in tumorigenesis and metastasis formation, together with the different response of tumor cells to the presence of this metal in comparison to healthy ones, can be targeted to develop novel selective anticancer drugs [20–22]. Copper, like iron, can be involved in the production of ROS by the Haber-Weiss reaction, the activation of redox cycles and the decrease of GSH, with consequent oxidative stress, which represent an alternative to platinum-induced DNA damage, hopefully leading to better selectivity [16,23]. We have recently disclosed a series of 2,3-dihydroxy- and 2-hydroxy-3-methoxy-benzaldehyde thiosemicarbazones (Fig. 1) and their copper(II) complexes that demonstrated a very promising anticancer profile: some of them, in fact, showed *in vitro* activity in the low nanomolar range [24]. Interestingly, mechanistic investigations allowed to highlight that these compounds can potently inhibit Protein Disulfide Isomerase (PDI), a copper-binding protein, that is emerging as a new therapeutic target for cancer treatment [25,26].

Overall, our previous results suggested that salicylaldehyde TSCs can represent a good starting point for the development of effective anticancer compounds; however, preliminary *in vivo* tests suffered of limitations due to poor solubility of the metal complexes [24]. The design of TSCs ligands with enhanced water-solubility is therefore a challenge of particular interest since this would allow further preclinical investigations. With these considerations in mind, we decided to introduce the sulfonic group to improve water solubility. Interesting cytotoxic properties have been already reported for some 5-sulfonate-salicylaldehyde TSCs, but the potential and the mechanism of action of their copper (II) complexes have been little explored [27–29].

Herein, we present the synthesis and characterization of five water-soluble sulfonated TSCs (**NaH_2L^1-NaH_2L^5**, Fig. 2) and of their corresponding copper(II) complexes **1–5**. In order to highlight the determinant role of the Cu(II) ion in the activity of the complexes, we also synthesized the complexes **6** and **7** (Fig. 2), with the Ni(II) and Zn(II) ions, which have quite different electronic characteristics and coordination geometries. The *in vitro* antitumor properties of **NaH_2L^1-NaH_2L^5** and **1–7** were assayed, both on 2D (HCT-15, 2008, PSN-1, A431, MCF-7, and MDA-MB-231 cells) and 3D (HCT-15 and 2008 cells) cancer cell cultures, and detailed investigations on their mechanism of action are also reported. *In vivo* preliminary studies performed in a model of solid tumor, the syngeneic murine Lewis Lung Carcinoma, by using the most promising complex **5** and cisplatin as the reference metallodrug, confirm the anticancer potential of this class of water-soluble copper(II) complexes.

2. Results and discussion

Synthesis. A first attempt to obtain the ligands **NaH_2L** [1]-**NaH_2L** [5] was performed by direct sulfonation of the pre-formed TSCs with an excess of concentrated H_2SO_4. However, this approach was abandoned, since the desired sulfonated TSCs could not be satisfactorily separated from the large amount of sodium sulfate obtained as a co-product of neutralization. Moreover, depending on the pH reached during the work-up, basic hydrolysis of the imine could occur. Therefore, a different strategy was considered (Scheme 1), following some literature suggestions [30]. Briefly, the parent 2,3-hydroxy or

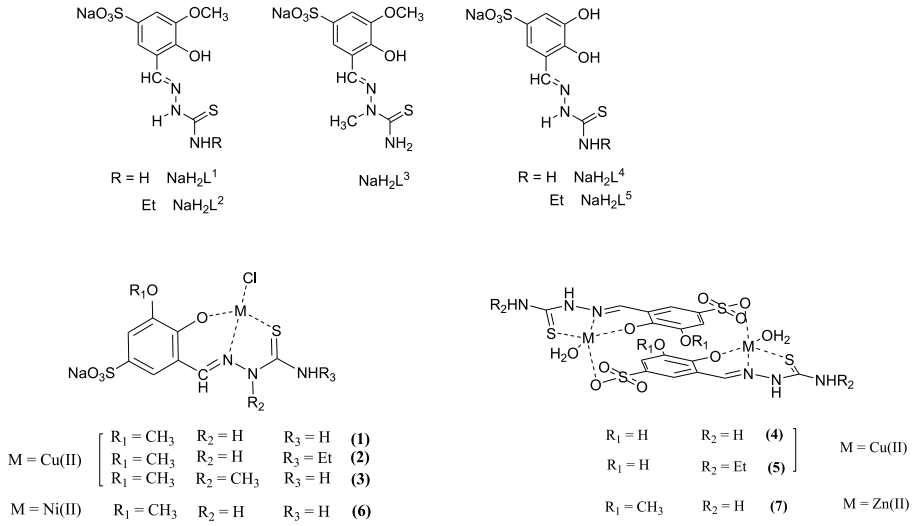

Fig. 2. Schematic representation of the ligands **NaH_2L^1-NaH_2L^5** and of the corresponding copper(II), nickel(II) and zinc(II) complex units in **1–7**; other possible coordinated water molecules are omitted.

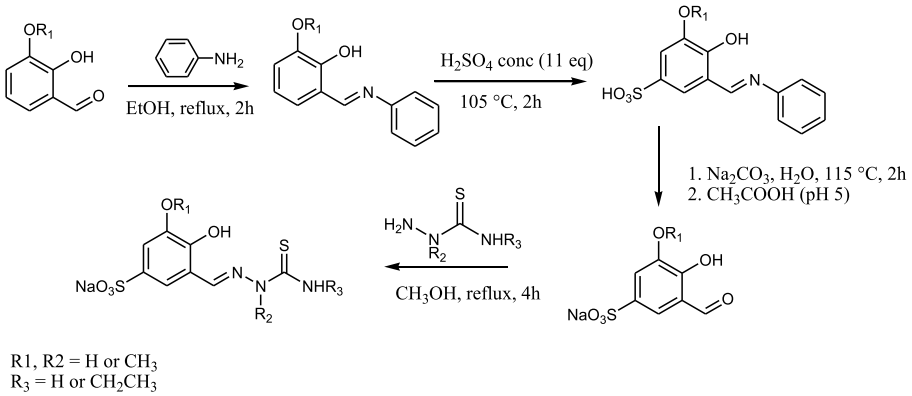

Scheme 1. Synthetic pathway followed for the synthesis of the water soluble TSCs **NaH_2L** [1]-**NaH_2L** [5].

2-hydroxy-3-methoxybenzaldehyde was condensed with aniline to obtain the corresponding Shiff base, which was subsequently sulfonated by reaction with an excess of concentrated sulfuric acid. The sulfonated Shiff base was isolated by precipitation and then hydrolyzed to obtain the sulfonated aldehyde (Scheme 1). Condensation reaction between 2, 3-dihydroxy-5-sulfonate or 2-hydroxy-3-methoxy-5-sulfonate benzaldehyde and the proper thiosemicarbazide led to the ligands **NaH_2L** [1]-**NaH_2L** [5] in good yields. They are formally triprotic (H_3L), but they were obtained as sodium salts; two acidic groups (O-H and thiosemicarbazone N-H) are present.

The ligands **NaH_2L** [1]-**NaH_2L** [5] were then characterized. In particular, it is possible to observe in their IR spectrum the presence of the absorbance relative to the sulfonate group at about 1045 and 1200 cm^{-1}. ^1H NMR spectrum registered in DMSO-d_6 highlighted that the ligands are in the *E* form in solution, as can be inferred from the chemical shift values of the HC=N and NH protons [28]. In the solid state the thione form is present, since there is no evidence, in the IR spectrum, of the S–H stretching band near 2600 cm^{-1} of the thiol tautomer; the N–H stretching band is clearly visible in the range 3130–3170 cm^{-1}.

The copper(II) complexes **1–5** (Fig. 2) were obtained by reacting $CuCl_2 2H_2O$ with **NaH_2L** [1]-**NaH_2L** [5] in methanol and adjusting the pH to 8–9 with NaOH to force the deprotonation of the ligand. The same procedure was adopted for the nickel(II) and zinc(II) complex **6** and **7**, by using $NiCl_2 6H_2O$ and $Zn(CH_3COO)_2\ 4H_2O$, respectively.

The complexes **1–7** were characterised by means of elemental analysis, FT-IR, ESI-MS, ICP-OES and, in the case of the zinc(II) diamagnetic complex **7**, by ^1H NMR spectroscopy. The comparison between the IR spectra of the free ligands and the complexes supports the hypothesis of a *O, N, S* tridentate coordination of the ligand. In the IR spectra of the complexes, in fact, the O-H stretching band around 3460 cm^{-1} disappears; furthermore, a shift of 15–60 cm^{-1} to higher frequency values for the C=N and C=S stretching bands suggests the involvement of these groups in the complexation. Interestingly, the copper(II) complexes **1**–**3** (with the 2-hydroxy-3-methoxy- ligands) and **4**–**5** (with the 2,3-dihydroxy ligands) have different compositions. In both cases, the copper (II) ion is coordinated by the tridentate TSC ligands, but **1**–**3** have the general formula $Cu(NaHL)Cl{\cdot}nH_2O$, while, for **4** and **5**, it is possible to propose a dimeric structure $[Cu(HL)(H_2O)]_2$, where the coordination sphere of the metal could be completed by a water molecule and the sulfonate moiety of an adjacent ligand (Fig. 2), as characterized by X-ray diffraction analysis for **5** and described in some cases in the literature [27–29]. This hypothesis is also corroborated by ICP-OES analysis: the percentage of Na^+ found in the monomeric complexes **1–3** is in line with what expected, while for the dimeric complexes **4** and **5** it is practically zero.

The ESI-MS spectra of the complexes **1**–**5** registered in methanol presented the peaks for the monometallic species $[CuL]^-$ and peaks corresponding to species with two copper ions (supporting information paragraph). ESI-MS analyses were also conducted dissolving **2** and **5** in NaCl aqueous solution (10 mM) and in this case weak peaks of the species $[Cu(HL)Cl]^-$ became visible (supporting information paragraph).

For the nickel(II) and zinc(II) complexes with **NaH_2L** [1], the analytical data are in accordance with the formula $[Ni(NaHL\ [1])Cl]{\bullet}3H_2O$ **(6)** and $[Zn(HL\ [1])]_2{\bullet}6H_2O$ **(7)** (Fig. 2).

After several attempts, crystals of **5** $[Cu(HL\ [5])(H_2O)]_2 2H_2O$ suitable for SC-XRD analysis were obtained from a methanol solution. In its crystal structure, **5** forms head-to-tail dimers in which the copper(II) ion, besides its square planar coordination obtained through the three donor atoms of the thiosemicarbazone and a water molecule, binds apically the negatively charged oxygen of the sulfonate moiety of a nearby molecule (Fig. 3).

This situation is not unusual with zwitterionic copper complexes containing the sulfonate moiety, and some examples can be found in the literature [27,28,31–33]. Since these are zwitterionic molecules it is reasonable to think that, during the crystal formation, once one molecule binds to the fragment of an adjacent one with the opposite charge, the probability that the other end finds the corresponding analogous with opposite charge in the same molecule is very high. An alternative way of packing would be the formation of polymeric chains but, in the case of sulfonated aromatic systems, very often this head-to-tail packing is also favoured by intermolecular π···π stacking interactions. In our specific case, in **5** the centroid···centroid contact is of 3.405 Å, indicating a strong interaction [34].

Interestingly, trying to obtain crystals of **2** suitable for X-ray diffraction, the species $[Cu(HL\ [2])(H_2O)_2]{\cdot}2H_2O$ was obtained (Fig. 4). Despite its close resemblance to compound **5**, the crystal structure of $[Cu(HL\ [2])(H_2O)_2]{\cdot}2H_2O$ contains more water molecules, and one of them, occupying the apical position in the copper coordination, prevents the formation of a head-to-tail dimer. We can speculate that this monomeric structure $[Cu(HL)(H_2O)_2]$ is an intermediate form between [Cu(NaHL)Cl], and the dimer $[Cu(HL)(H_2O)]_2$, as characterized in **5**. In $[Cu(HL\ [2])(H_2O)_2]{\cdot}2H_2O$ the hydrogen bond pattern involving the water molecules is rather complex. The water molecule coordinated in the apical position of copper connects three nearby molecules bridging two complexes with

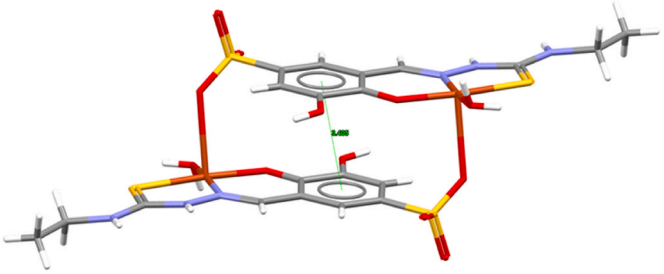

Fig. 3. Crystal structure of complex **5** obtained by X-ray diffraction analysis.

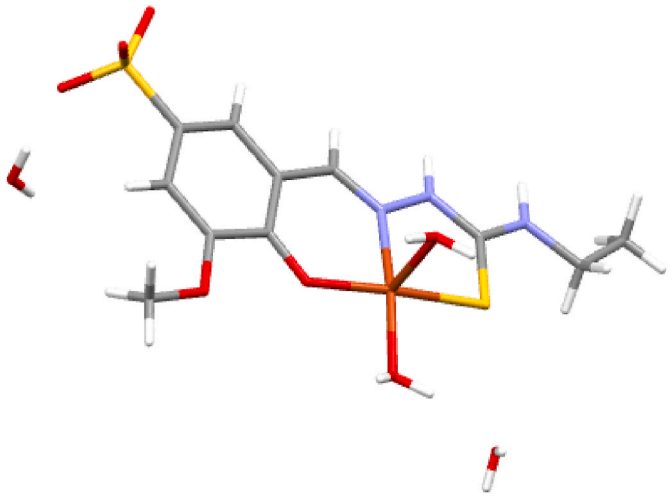

Fig. 4. Crystal structure of [Cu(HL [2])$(H_2O)_2$]·$2H_2O$.

sulfonate oxygens acting as an H donor, and forms a third hydrogen bond, as an acceptor, with the terminal NH of a third complex. The water molecule bonded to copper and lying in the coordination plane binds to two crystallization water molecules through its hydrogens. One of the two remaining crystallization waters bridges the equatorial water with a sulfonate oxygen and the other one acts also as a donor with the oxygen of the methoxy group of an adjacent complex.

Evidently, these complexes are prone to rearrangements in solution. In fact, also during the recrystallization of **1** some dark green crystals were isolated that from SC-XRD analysis resulted to be [Cu(HL [1])$(H_2O)]_2 2H_2O$, with a structure based on head-to-tail dimers (Fig. S13) as in **5**. The only significant difference between the structures of **5** and [Cu(HL [1])$(H_2O)]_2 2H_2O$ is that in this case the intermolecular π···π interaction is rather weak (centroid···centroid contact about 4 Å).

Before carrying out the biological tests, the stability of the complexes **1–7** in solution was evaluated over 72 h, by recording their UV spectra (C ≈ 40–50 μM) in 25 mM of Hepes buffer solutions at pH = 7.4 in H_2O/NaCl 0.9 %. In Fig. S14 the UV–visible spectra for **1** and **4** are reported. The spectra of the 2-hydroxy-3-methoxy derivatives **1–3** did not change over 72 h, while the absorbance bands of the 2,3-dihydroxy derivatives **4** and **5** displayed slight shifts over time (Fig. S14). We wondered if the presence of NaCl in solution could originate such variations, being involved in the rearrangements between monomer [Cu(NaHL)Cl] and dimer $[Cu(HL)(H_2O)]_2$ forms. We therefore registered the UV–visible spectra of **4** and **5** in Hepes buffer solution (25 mM, pH = 7.4) in absence of NaCl (Fig. S15). In this case, effectively, no visible variations were observable in the UV–visible spectra over 72 h.

Effects on cell viability. The *in vitro* anticancer potential of the newly developed complexes and of the free sulfonated TSC ligands has been evaluated on six different human cancer cell lines including HCT-15 (colorectal), 2008 (ovarian), PSN-1 (pancreatic), A431 (cervical), MCF-7 as well as MDA-MB-231 (breast) cancer cells. For comparison purposes, the efficacy of the milestone of metal-based drugs, cisplatin, was assessed under the same experimental conditions. The cytotoxicity parameters, expressed in terms of IC_{50} and obtained after 72 h of drug exposure by MTT assay, are reported in Table 1.

The uncomplexed TSCs **NaH_2L^1** [1]- **NaH_2L^5** [5] were completely ineffective against all tested cancer cell lines. Similarly, both Ni(II) and Zn(II) complexes **6** and **7** did not affect cancer cell viability towards the in-house cancer cell panel. Conversely, copper(II) derivatives showed a remarkable cytotoxicity against exposed cancer cell lines, with average IC_{50} values in the low/sub-micromolar range. Interestingly, MDA-MB-231 triple negative breast cancer cells, characterized by low sensitivity to cisplatin, exhibited remarkably greater sensitivity to all TSC copper(II) complexes, and these results are very promising,

Table 1
2D cytotoxic activity of the TSCs ligands and their metal complexes **1–7**.

IC_{50} (μM) ± S.D.						
	HCT-15	2008	PSN-1	A431	MCF-7	MDA-MB-231
NaH_2L^1	>100	>100	>100	>100	>100	>100
NaH_2L^2	>100	>100	>100	>100	>100	>100
NaH_2L^3	>100	>100	>100	>100	>100	>100
NaH_2L^4	>100	>100	>100	>100	>100	>100
NaH_2L^5	>100	>100	>100	>100	>100	>100
(1)	5.9 ± 0.8	8.1 ± 2.8	4.7 ± 1.4	8.3 ± 1.1	4.1 ± 1.0	7.2 ± 1.1
(2)	6.4 ± 1.9	9.2 ± 1.1	6.5 ± 2.2	9.8 ± 1.4	8.3 ± 0.2	8.1 ± 1.3
(3)	6.0 ± 1.1	6.9 ± 1.1	5.4 ± 0.4	4.5 ± 0.8	8.9 ± 0.4	6.3 ± 1.7
(4)	0.3 ± 0.1	7.5 ± 0.3	4.1 ± 0.9	2.9 ± 1.2	1.3 ± 0.4	5.4 ± 1.1
(5)	0.9 ± 0.3	6.2 ± 1.5	1.8 ± 0.7	1.8 ± 0.4	1.7 ± 1.0	2.6 ± 0.3
(6)	>100	>100	>100	>100	>100	>100
(7)	>100	>100	>100	>100	>100	>100
Cisplatin	13.9 ± 1.6	2.1 ± 1.3	12.1 ± 2.8	2.0 ± 0.8	8.8 ± 0.2	30.5 ± 2.6

Cells (3–5 x 10^3 cell/well) were treated for 72 h with tested compounds. Cell viability was estimated by means of the MTT test. The IC_{50} values were calculated by a four-parameter (4-PL) logistic model ($p < 0.05$). S.D. = standard deviation.

considering the aggressive behaviour of the triple-negative BC subtype. **4** and **5** were the most active copper-based TSC complexes in 2D assays, with average IC_{50} values of 3.6 and 2.5 μM, respectively. Remarkably, compound **5** was about 12 and 15 times more effective than cisplatin against MDA-MB-231 triple negative breast and HCT-15 colorectal human cancer cells, respectively. Even though to a lower extent, also complexes **1–3** demonstrated a prominent cytotoxic potential, with complexes **1** and **2** being on average about 1.8 times more effective than cisplatin (average IC_{50} values of 6.4, 6.3 and 11.6 μM for **1**, **2** and cisplatin, respectively).

Considering these very promising results and keeping in mind that drug resistance represents a crucial issue in anticancer therapy [35], we also assessed the ability of **1**–**5** to bypass acquired drug resistance. In particular, they were evaluated for their antiproliferative activity against human colon cancer cells selected for their sensitivity/resistance to oxaliplatin (LoVo/LoVo OXP cells) or belonging to the multi-drug resistance (MDR) phenotype (LoVo MDR cells). Table 2 shows the degree of resistance in terms of the resistant factor (RF), which is defined as the ratio between IC_{50} (obtained using MTT assay after 72 h of drug exposure) calculated for the resistant cells and those for the sensitive ones. As previously reported, LoVo OXP cells were about 13-fold more resistant to oxaliplatin than parental cells [36]. All TSCs copper(II)

Table 2
Cytotoxic activity of **1–7** towards LoVo, LoVo OXP and LoVo MDR cell lines. Resistance factor (RF) is indicated in parenthesis.

IC_{50} (μM) ± S.D. (RF)			
	LoVo	LoVo OxPt	LoVo MDR
(1)	5.0 ± 0.7	2.5 ± 0.9 (0.5)	1.2 ± 0.2 (0.2)
(2)	7.3 ± 0.9	6.2 ± 1.4 (0.9)	2.4 ± 0.8 (0.3)
(3)	5.8 ± 1.1	2.7 ± 0.9 (0.5)	10.4 ± 0.5 (1.8)
(4)	0.7 ± 0.1	1.8 ± 0.6 (2.7)	0.7 ± 0.2 (1.0)
(5)	1.3 ± 0.2	0.9 ± 0.2 (0.7)	0.4 ± 0.2 (0.3)
Oxaliplatin	1.4 ± 0.3	19.3 ± 1.7 (13.7)	1.4 ± 0.8 (1.0)
Doxorubicin	1.1 ± 0.3	–	19.2 ± 2.4 (17.3)

Cells (5 × 10^3 well) were treated for 72 h with the tested compounds. Cell viability was measured by means of MTT test. IC_{50} values were calculated using the 4-PL logistic model ($p < 0.05$). S.D. = standard deviation. RF = IC_{50} (resistant cells)/IC_{50} (wild-type cells).

complexes were equally effective against sensitive (LoVo) and resistant (LoVo OXP) colon cancer cells and possessed RFs much lower than those calculated for oxaliplatin and doxorubicin, thus attesting their ability to overcome both oxaliplatin and MDR resistances.

To preliminarily assess cell selectivity profile of the Cu(II) complexes **1–5**, we also evaluated their cytotoxic potential against noncancerous human HEK293 cells (Table 3). IC_{50} values calculated for all tested complexes were significantly higher than those obtained (on average) against tumour cells. Noticeably, selectivity index values (S.I. = the quotient of the average IC_{50} toward normal cells divided by the average IC_{50} for the malignant cells) obtained with compounds **4** and **5** were roughly 13 and 23 times higher than that calculated for cisplatin, thus indicating for this class of metal complexes an outstanding preferential cytotoxicity against cancer cells.

Although 2D cell cultures are widely employed for *in vitro* screening due to their low cost, simplicity, and reliability, they are unable to properly mimic the properties of *in vivo* tumors. In contrast, 3D cell cultures, offering greater efficiency in reproducing the heterogeneity and complexity of the tumor microenvironment, enable the study of tumor response to anticancer drugs in a more physiologically relevant context, and therefore are more predictive of *in vivo* outcomes [37].

On these bases, the cytotoxicity of **1**–**5** was also examined using 3D cell culture models of human colon (HCT-15) and ovarian (2008) cancers. Cancer cell spheroids were treated for 72 h with the investigated compounds, and cell viability was assessed by means of a modified acid phosphatase (APH) assay (Table 4). As expected, cells in 3D cultures, after forming the spheroids, were more resistant to drug treatment compared to those cultivated in a single layer in 2D. Nevertheless, against the LoVo colorectal cancer 3D model, TSC copper(II) complexes were much more effective (up to 8-fold) than cisplatin, confirming once again that human colorectal cancer cells are highly sensitive to copper complexes [36]. Against 2008 human ovarian 3D cancer cell models, only complexes **1**, **4** and **5** were much more effective than the reference drug. Overall, similarly to 2D monolayer cell culture experiments, **4** and **5** emerged as the most promising compounds, with IC_{50} values in the low-micromolar range.

Mechanistic studies. To correlate cytotoxic activity with intracellular accumulation of the metal ion, cancer cell uptake experiments were performed in HCT-15 colorectal cancer cells. Cells were treated for 24 h with 3 μM of copper(II) complexes **1–5**. The intracellular copper amount was quantified by means of graphite furnace atomic absorption spectrometry (GF-AAS) analysis, and the results, expressed as μg of metal per 10^6 cells, are shown in Fig. 5. Although at a different extent, all Cu(II) complexes were able to effectively accumulate into LoVo colorectal cancer cells.

By plotting copper cellular amount against IC_{50} values calculated from 2D monolayer cultures, a linear correlation between copper cellular uptake and cytotoxicity could be drawn for all the Cu(II) derivatives: cellular copper accumulation is confirmed as a key determinant in modulating the *in vitro* antitumor activity of the TSC-based copper(II) complexes.

Table 3
IC_{50} for complexes **1**–**5** towards HEK293 cells, with indication of the selectivity index (S.I.).

IC_{50} (μM) ± S.D.		
	HEK 293	S.I.
(1)	51.7 ± 5.0	8.2
(2)	62.8 ± 3.2	7.8
(3)	58.0 ± 6.4	9.2
(4)	111.6 ± 15.6	31
(5)	137.5 ± 10.8	55
Cisplatin	24.7 ± 0.9	2.4

Cells (5 × 10^3 well) were treated for 72 h with the tested compounds. Cell viability was measured by means of a MTT test. IC_{50} values were calculated using the 4-PL logistic model ($p < 0.05$). S.D. = standard deviation. SI = IC_{50} toward normal cells/average IC_{50} toward malignant cells (Table 1).

Table 4
Cytotoxicity of the copper(II) complexes **1**–**5** towards 3D cell culture models.

IC_{50} (μM) ± S.D.		
	HCT-15	2008
(1)	19.3 ± 2.9	11.5 ± 2.9
(2)	37.4 ± 4.8	20.5 ± 5.8
(3)	17.8 ± 1.3	18.4 ± 0.3
(4)	8.1 ± 0.8	6.3 ± 1.6
(5)	15.1 ± 0.2	8.9 ± 1.3
Cisplatin	68.2 ± 4.6	13.3 ± 0.9

Cells (2.5 × 10^3 x well) were treated for 72 h with tested compounds. Cell viability was estimated by means of the APH test. IC_{50} values were calculated from the dose-response curves by a 4-PL model ($p < 0.05$). S.D. = standard deviation.

During the past three decades, research studies exploring the mechanism of action of copper(II) complexes have proposed several different molecular targets and, among them, PDI has recently emerged as a potential target for several copper(I) and (II) complexes as well as for TSCs [24–26]. On this basis, we also evaluated the ability of the newly synthesized complexes to act as PDI inhibitors, in analogy to our previous studies with the non-sulfonated parent compounds [24]. PDI enzyme was treated with 10 or 20 μM of tested complexes, and the ability to hamper its activity was assessed by a biochemical colorimetric method (Proteostat kit). As shown in Fig. 6A, copper derivatives **1**–**5** were able to inhibit PDI in a dose dependent manner. At the highest tested dose, compounds **1**, **4** and **5** were able to reduce PDI catalytic activity by about 80 %. IC_{50} value calculated for complex **4** is 5.5 μM (Fig. 6A, right).

As it is well-known that one of the key cellular functions of PDI is to catalyse the reduction of disulfide bonds and the oxidation of thiols, we evaluated the levels of reduced thiols in HCT-15 colorectal cells treated with complexes **1–5** (Fig. 6B). Interestingly, cells treated for 36 h with 5 μM of the tested complexes showed an outstanding increase in total sulfhydryl content, which reached 146 % with complex **5** treated cells. (Fig. 6B). Accordingly, no ROS generation were detected in HCT-15 cancer cells following treatment treated with 25 μM of Cu(II) complexes (Fig. 6C). All together these results support the hypothesis that the TSC copper(II) derivatives are able to effectively target PDI in colon cancer cells causing an imbalance in cell redox homeostasis by shifting it towards a more “reduced state”.

PDIs are abundant endoplasmic reticulum (ER)-resident oxidoreductases that, being implicated in disulfide bonds formation, play a crucial role in protein folding. However, due the major crosstalk existing between ER and mitochondria in redox homeostasis, PDI inhibition has been shown to strongly affect mitochondrial patho-physiological stability [38]. On this basis, we also evaluated mitochondrial membrane polarization of human HCT-15 colon cancer cells exposed to tested complexes (Fig. 7A). Carbonyl cyanide *m*-chlorophenyl hydrazone (CCCP), a chemical inhibitor of the oxidative phosphorylation, was used as positive control. Interestingly, treatment with **1**–**5** did not induce a mitochondrial depolarization, but rather a slight hyperpolarization was underlined following treatment with the copper complexes **3**.

Additional detailed morphological analyses performed both by transmission electron microscopy (Fig. 7B) and by phase contrast microscopy (Fig. 7 D) studies revealed that treatment of HCT-15 cells with IC_{50} doses of complexes **4** and **5** for 24 h induce a massive ER cisternae enlargement, which is a clear sign of ER stress, and a concomitant cytoplasmic vacuolization. Furthermore, a slight increase in mitochondrial dimension (swelling) associated with a decreased electron density of the inner membrane and matrix regions as well as alteration of cristae features were detected (Fig. 7B). Conversely, no signs of nuclear modification, chromatin condensation or cell shrinking were evidenced. Accordingly, HCT-15 cells treated for 48 h with IC_{50} doses of tested complexes and stained with Hoechst 33,258 fluorescent probe did not

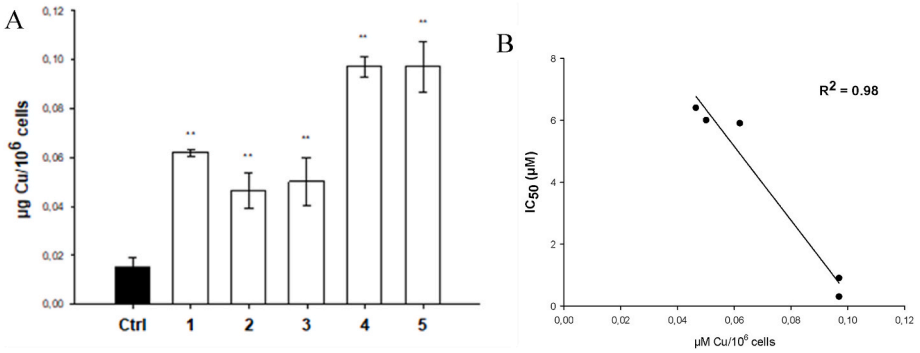

Fig. 5. Cellular uptake studies (A) and correlation between copper content and cytotoxicity (B). HCT-15 cells were treated for 24 h with 3 µM copper(II) complexes **1–5**, and the intracellular copper amount was estimated using GF-AAS analysis. Error bars indicate the standard deviation. **p < 0.01 compared with the control.

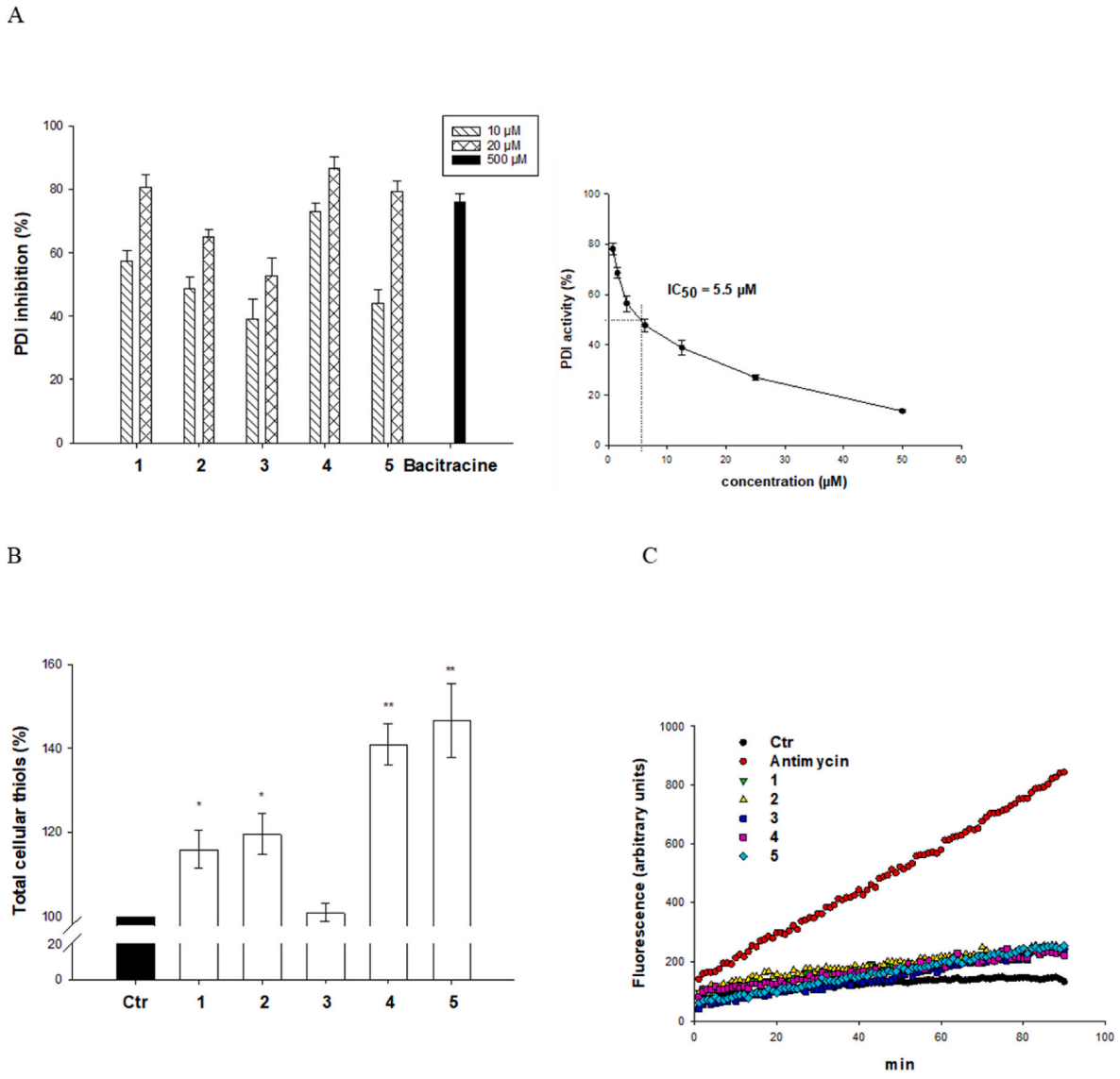

Fig. 6. A) Cell-free inhibition of PDI. PDI inhibition induced by **1**–**5** was measured by Proteostat PDI assay kit. The PDI inhibitor Bacitracine (0.5 mM) was used as a positive control. Error bars indicate S.D. On the right, dose-response curve for PDI inhibition for compound **4** with indication of the IC_{50} value. (B) Sulfhydryl content in HCT-15 cancer cells incubated for 36 h with 5 µM of tested compounds. The sulfhydryl group amount was determined by the DTNB assay. Error bars indicate S.D. *p < 0.05 compared with control. (C) ROS production. HCT-15 cells were preincubated in PBS/10 mM glucose medium for 20 min at 37 °C in the presence of 10 µM CM−H_2DCFDA and then treated with the tested compounds at 25 µM. Antimycin (3 µM), a well-known inhibitor of mitochondrial Complex III in the respiratory chain, was used as positive control.

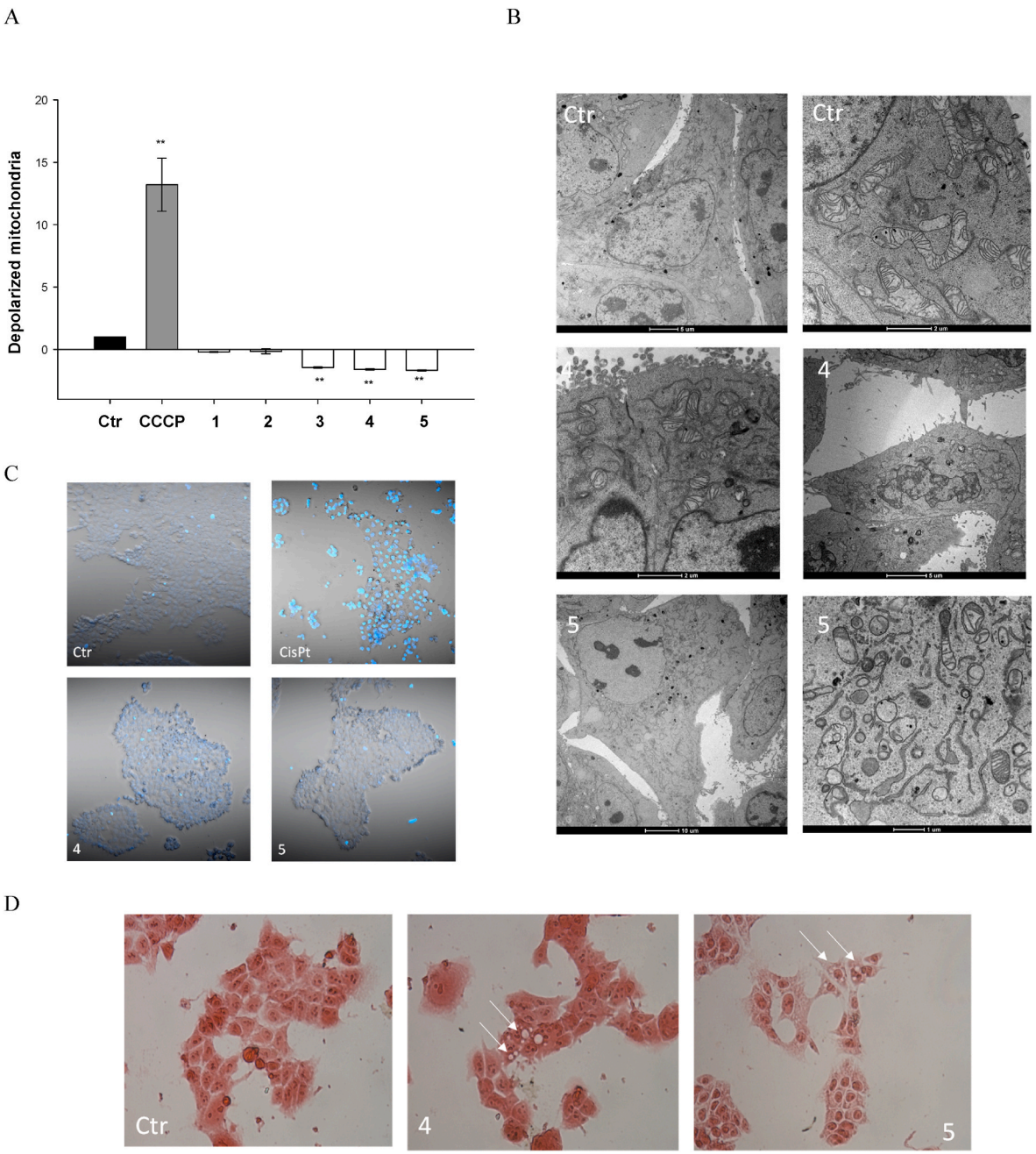

Fig. 7. Mitochondrial depolarization (A) and morphological analysis (B–D). A. HCT-15 cells were treated for 24 h with increasing concentrations of the tested complexes or CCCP (3 μM). The percentage of cells with depolarized mitochondrial membrane potential was determined by Mito-ID® Membrane Potential Kit. Error bars indicate S.D. **$p < 0.01$. (B) TEM analysis of HCT-15 colon cancer cells untreated (ctr) or treated for 24 h with IC_{50} of complexes **4** or **5**. (C) Hoechst staining of untreated (ctr) HCT-15 cells or incubated for 48 h with IC_{50} doses of cisplatin, complexes **4** or **5** (10 × magnification). (D) Phase contrast images of HCT-15 cells stained with hemeatoxylin and eosin: control cells (ctr) or cells treated with IC_{50} of complexes **3** or **4** for 24 h (40 × magnification).

show any classical sign of apoptosis induction (*e.g.* brightly stained nuclei, chromatin condensation and fragmentation), which were unlike evident on colorectal cells treated with the reference metallo-drug cisplatin (Fig. 7C).

Altogether these results suggest the induction of a cancer cell death mechanism different from apoptosis, called paraptosis or, as more recently renamed, cuproptosis [39], that is strongly correlated to the induction of ER stress and of the Unfolded Protein Response (UPR).

***In vivo* preliminary studies.** Due to the high potential demonstrated by **1**–**5**, we thought of interest to validate their antitumor potential in preclinical translational studies. To this aim, based on a distinct cell selectivity profile and high cytotoxicity both on 2D and 3D cancer cell culture systems, we selected compound **5** for further profiling. We performed preliminary *in vivo* anticancer investigations in a model of solid tumor, the highly aggressive syngeneic murine Lewis Lung Carcinoma (LLC). Tumor growth inhibition induced by **5** (5 mg kg^{-1}) was compared with that promoted by cisplatin (3 mg kg^{-1} in saline solution). Chemotherapy doses were based on preliminary experiments to determine the maximum tolerated dose that did not induce excess weight loss or toxicity. Seven days after tumor inoculation, tumor-bearing mice were randomized into vehicle (water) control and treatment groups. The tumor growth was estimated at day 15 and the results are reported in Table 5. As an estimation of the adverse side effects, changes in the body weights of tumor-bearing mice were monitored every two days starting

Table 5
In vivo antitumor activity. LLC was implanted i.m. in C57BL mice. After 24 h from tumor implantation, mice were randomly divided into groups of 8 animals (10 controls). Chemotherapy was delayed until the tumor was visible (day 7). Day 15: animals were sacrificed, and tumor growth inhibition was determined as the difference in weight of the tumor-bearing leg and the healthy leg (%), referred to control animals. [a]vehicle (water).

	Daily dose ($mg \cdot kg^{-1}$)	Average tumor weight (mean ± S.D., g)	Inhibition of tumor growth (%)
control[a]	–	0.487 ± 0.09	–
5	5	0.081 ± 0.03[a]	83.4
cisplatin	3	0.096 ± 0.03[a]	80.3

[a] $p < 0.1$.

from day 7 (Fig. S16).

Noteworthy, administration of **5** at 5 mg kg^{-1} induced a 83.4 % reduction of the tumor mass, therefore attesting an antitumor efficacy slightly higher than that elicited by cisplatin dosed at 3 mg kg^{-1}. Moreover, the time course of body weight changes attested that cisplatin induced elevated anorexia (Fig. S16), whereas the treatment with **5** did not induce a significant body weight loss (<10 %) during the entire experimentation, thus suggesting for the TSC Cu(II) derivative a better tolerability profile with respect to the reference metallodrug.

3. Conclusions

It has been clearly demonstrated that even minimal variation on the ligand can lead, in the corresponding metal complex, to a very different cytotoxic activity. In our previous studies, the introduction of a substituent (OH or methoxy group [40]) in *ortho* to the salicylic OH of the salycilhydrazone TSCs, led to obtaining TSCs and related copper(II) complexes with cytotoxic activity in the nanomolar range: one of these complexes was about 3000 times more active than cisplatin against human pancreatic and colon cancer cell lines (PSN1 and HCT-15 lines) [24]. However, *in vivo* tests have shown that the poor solubility of these complexes severely limits their prospects. It was then decided to increase the solubility by sulfonating the previously obtained ligands, separating them in the form of **NaH_2L^1-NaH_2L^5** salts. **NaH_2L^1-NaH_2L^5** and their respective complexes **1**–**7** were indeed very soluble in physiological solutions. Cytotoxicity studies revealed that **NaH_2L^1-NaH_2L^5** were completely inactive against the tested cell lines, contrary to their non-sulfonated counterparts. Concerning to the corresponding copper (II) complexes, compounds **1**–**5**, although less active than Cu(II) complexes bearing the non-sulfonated ligands, showed a cytotoxic potency still in the low micromolar range, both in 2D and 3D cancer cell cultures, being highly effective also against cancer cells with intrinsic or acquired resistance to platinum drugs [35]. Noteworthy, moving from non-sulfonated Cu(II) complexes to **1**–**5,** an outstanding preferential cytotoxicity against cancer cells was obtained. It was quite reasonable to expect that **NaH_2L** [1]-**NaH_2L** [5] can hardly cross cell membrane, and thus they can be scarcely cytotoxic, whereas **1–5** copper(II) complexes, being overall neutral, are more lipophilic, allowing them to efficiently accumulate into monolayer cancer cells as well as to penetrate cancer 3D spheroids. As a whole, biological tests evidenced a key role for copper(II) ion in increasing TSC metal complex cytotoxic potential. Complexes **6** and **7**, where Ni(II) and Zn(II) ions replace Cu(II), did not affect cancer cell viability. Moreover, in treated cancer cells, a linear correlation between copper cellular uptake and cytotoxic activity was found. Cellular mechanistic studies led to the identification of PDI as one of the crucial cellular targets of this class of copper(II) complexes with TSCs ligands. By hampering PDI activity, copper(II) complexes **1–5** were able to cause an imbalance in cancer cell redox homeostasis thus leading to cancer cell death via cuproptosis, a copper-dependent kind of cell death which added to ferroptosis [39] among programmed cell deaths dependent on a metal ion accumulation. Preliminary *in vivo* studies, performed on a highly aggressive murine solid tumor model, attested for the most representative water-soluble copper complex **5** an equal *in vivo* antitumor efficacy and a better tolerability profile with respect to those elicited by the reference metallodrug. Taken together our data highlights the very promising anticancer potential of this novel class of sulfonated TSCs copper(II) complexes acting as PDI-targeting species.

4. Experimental

Materials and methods. Chemistry. Commercial reagents were purchased from Sigma-Aldrich. The purity of the synthesized compounds was determined by elemental analysis and verified to be ≥ 95 %. ^{1}H NMR spectra were recorded at 25 °C on a Bruker Avance 400 FT spectrophotometer. The ATR-IR spectra were recorded by means of a Nicolet-Nexus (Thermo Fisher) spectrophotometer by using a diamond crystal plate in the range of 4000-400 cm^{-1}. Elemental analyses were performed by using a CHNS FlashSmart Thermo Fisher analyzer with gas-chromatographic separation. Electrospray mass spectral analyses (ESI-MS) were performed with an electrospray ionization (ESI) time-of-flight Micromass 4LCZ spectrometer. Samples were dissolved in methanol. The UV–vis spectra were collected using a Thermo Evolution 260 Bio spectrophotometer provided with a thermostatting Peltier device, and quartz cuvettes with 1 cm path length.

ICP-AES analysis (Inductively Coupled Plasma – Atomic Emission Spectroscopy) was performed as follows: 5 mg of solid sample were suspended in 5 mL of HNO_3 65 % and 1 mL of H_2O_2 30 %, then digested in a *Milestone* microwave MLS-1200 MEGA (digestion sequence: 1 min at 250 Watt, 1 min at 0 Watt, 5 min at 250 Watt, 5 min at 400 Watt, 5 min at 650 Watt, 5 min of cooling). The solutions were diluted to 50 mL with bi-distilled water and analyzed by using an emission spectrometer JY 2501 with coupled plasma induction in radial configuration HORIBA Jobin Yvon (Kyoto, Japan), ULTIMA2 model. Instrumental features: monochromator Model JY 2501; focal length 1 m; resolution 5 p.m.; nitrogen flow 2 l/min. ICP source: nebulizer Meinhard, cyclonic spraying chamber; argon flow 12 l/min; wavelengths range 160–785 nm; optical bench temperature 32 °C. The wavelength used for quantitative analysis was chosen by examining the emission line with greater relative intensity, ensuring that there was no spectral interference with the Argon emission lines. Acquisition parameters: wavelength Cu (nm): 224.700; Voltage (V): 580; Gain: 100; wavelength Na (nm): 588.995; Voltage (V): 570; Gain: 10. The quantitative analysis was performed after the acquisition of a calibration line using standard solutions in HNO_3 10 %, to simulate the final acidity of the samples; the concentration range of the standards varied from 0.5 mg/L to 100 mg/L. Data acquisitions and processing were performed using the ICP JY v 5.2 software (Jobin Yvon).

General synthesis of NaH_2L [1]-**NaH_2L** [5]. The thiosemicarbazone ligands were synthesized by condensation of the proper thiosemicarbazide with an equimolar amount of 5-sulfonate-2-hydroxy-3--methoxybenzaldehyde or 5-sulfonate-2,3-dihydroxybenzaldehyde sodium salt in methanol at 85 °C for 4 h according to procedures previously reported [24–26]. The synthesis of **NaH_2L** [4] and **NaH_2L** [5] was performed under nitrogen, to avoid oxidation side-reactions of the catechol moiety. The water-soluble 5-sulfonate aldehydes were obtained by a 3-steps procedure, as illustrated in Scheme 1 (see supporting information paragraph for details) [30].

Sodium 2-hydroxy-3-methoxy-5-sulfonate-benzaldehyde-3-thiosemicarbazone (NaH_2L* [1]*). Beige powder. Yield = 53 %. IR (ATR, cm^{-1}): $\nu(NH_2)+\nu(OH) = 3384$; $\nu(NH) = 3173$; $\nu(C{=}N) = 1609$; $\nu(C{=}S) = 1257$; $\nu(SO_3) = 1104, 1038$. ^{1}H NMR (400 MHz, DMSO, 25 °C) δ 11.41 (b, 1H, NH), 9.38 (b, 1H, OH), 8.40 (s, 1H, CH=N), 8.11 (b, 1H, NH), 7.71 (b, 1H, NH), 7.60 (d, $J = 1.9$ Hz, 1H, CH_{arom}), 7.16 (d, $J = 1.9$ Hz, 1H, CH_{arom}), 3.81 (s, 3H, OCH_3). ^{13}C NMR (101 MHz, DMSO, 25 °C) δ 177.7, 146.9, 146.2, 140.5, 139.7, 119.1, 115.6, 110.4, 55.9. ESI-MS (negative ions, *m/z*): 304.3 $(M - Na)^-$. Elemental analysis calculated for $C_9H_{10}N_3NaO_5S_2 \cdot H_2O$: C 31.30, H 3.50, N 12.17, S 18.57. Found: C 31.56, H 3.17, N 12.17, S 18.98.

Sodium 2-hydroxy-3-methoxy-5-sulfonate-benzaldehyde-4-ethyl-3-thiosemicarbazone (NaH$_2$L* [2]*). White powder. Yield = 57 %. IR (ATR, cm^{-1}): ν(OH) = 3384; ν(NH) = 3173; ν(C=N) = 1609; ν(C=S) = 1257; ν(SO$_3$) = 1104, 1038. ^{1}H NMR (400 MHz, DMSO, 25 °C) δ 11.35 (s, 1H, NH), 9.37 (b, 1H, OH), 8.41 (s, 1H, CH=N), 8.33 (t, J = 6.0 Hz, 1H, NH), 7.63 (d, J = 1.9 Hz, 1H CH$_{arom}$), 7.17 (d, J = 1.9 Hz, 1H, CH$_{arom}$), 3.81 (s, 3H, OCH$_3$), 3.58 (p, J = 6.9 Hz, 2H, CH$_2$), 1.14 (t, J = 7.1 Hz, 3H, CH$_3$). ^{13}C NMR (101 MHz, DMSO, 25 °C) δ 176.5, 146.8, 146.1, 140.0, 139.6, 119.4, 115.6, 110.4, 55.9, 18.6, 14.7. ESI-MS (negative ions, m/z): 332.2 (M − Na)$^-$. Elemental analysis calculated for $C_{11}H_{14}N_3S_2O_5Na$: C 37.17, H 3.97, N 11.82, S 18.05. Found: C 37.08, H 4.30, N 11.19, S 18.11.

Sodium 2-hydroxy-3-methoxy-5-sulfonate-benzaldehyde-3-methyl-thiosemicarbazone (NaH$_2$L* [3]*). Beige powder. Yield = 53 %. IR (ATR, cm^{-1}): ν(OH)+ν(NH$_2$) = 3452, 3323; ν(C=N) = 1574; ν(C=S) = 1274; ν(SO$_3^-$) = 1180, 1051. ^{1}H NMR (400 MHz, DMSO, 25 °C) δ 9.60 (s, 1H, OH), 8.43 (b, 1H, NH), 8.06 (s, 1H, CH=N), 7.88 (s, 1H, NH), 7.65 (d, J = 1.9 Hz, 1H, CH$_{arom}$), 7.19 (d, J = 1.9 Hz, 1H, CH$_{arom}$), 3.83 (s, 1H, CH$_3$), 3.76 (s, 1H, CH$_3$). ^{13}C NMR (101 MHz, DMSO, 25 °C) δ 180.5, 147.0, 146.4, 139.7, 137.7, 119.4, 115.5, 110.4, 55.9, 32.6. ESI-MS (negative ions, m/z): 318.3 (M − Na)$^-$. Elemental analysis calculated for $C_{10}H_{12}N_3NaO_5S \cdot 1.5H_2O$: C 32.61, H 4.10, N 11.41, S 17.41. Found: C 32.28, H 4.00, N 10.80, S 17.41.

Sodium 2,3-dihydroxy -5-sulfonate-benzaldehyde-3-thiosemi carbazone (NaH$_2$L* [4]*). White powder. Yield = 46 %. IR (ATR, cm^{-1}): ν(OH)+ν(NH$_2$) = 3462, 3285; ν(NH) = 3193; ν(C=N) = 1617; ν(C=S) = 1237; ν(SO$_3$) = 1177, 1041. ^{1}H NMR (400 MHz, DMSO, 25 °C) δ 11.37 (s, 1H, NH), 9.61 (b, 1H, OH), 9.10 (b, 1H, OH), 8.36 (s, 1H, CH=N), 8.09 (b, 1H, NH), 7.68 (b, 1H, NH), 7.42 (d, J = 2.0 Hz, 1H, CH$_{arom}$), 7.12 (d, J = 2.0 Hz, 1H, CH$_{arom}$). ^{13}C NMR (101 MHz, DMSO, 25 °C) δ 177.6, 145.5, 144.6, 141.3, 139.5, 119.2, 114.7, 114.4. ESI-MS (negative ions, m/z): 290.3 (M − Na)$^-$. Elemental analysis calculated for $C_8H_8N_3NaO_5S_2 \cdot H_2O$: C 29.00, H 3.04, N 12.68, S 19.36. Found: C 28.92, H 3.19, N 12.29, S 19.76.

Sodium 2,3-dihydroxy-3-methoxy-5-sulfonate-benzaldehyde-4-ethyl-3-thiosemicarbazone (NaH$_2$L* [5]*). Beige powder. Yield = 52 %. IR (ATR, cm^{-1}): ν(OH) = 3329; ν(NH) = 2974; ν(C=N) = 1615; ν(C=S) = 1284; ν(SO$_3$) = 1175, 1047. ^{1}H NMR (400 MHz, DMSO, 25 °C) δ 11.32 (b, 1H, NH), 9.4 (b, 2H, OH), 8.37 (s, 1H, CH=N), 8.30 (t, J = 5.9 Hz, 1H, NH), 7.45 (d, J = 2.0 Hz, 1H, CH$_{arom}$), 7.12 (d, J = 2.0 Hz, 1H, CH$_{arom}$), 3.58 (p, J = 6.9 Hz, 2H, CH$_2$), 1.13 (t, J = 7.1 Hz 3H, CH$_3$). ^{13}C NMR (101 MHz, DMSO, 25 °C) δ 176.4, 145.4, 144.5, 140.9, 139.5, 119.3, 114.6, 114.3, 38.4, 14.7. ESI-MS (negative ions, m/z): 332.2 (M − Na)$^-$. Elemental analysis calculated for $C_{10}H_{12}N_3NaO_5S_2 \cdot H_2O$: C 33.42, H 3.93, N 11.69, S 17.85. Found: C 33.08, H 3.90, N 11.23, S 18.08.

General synthesis of the copper(II) complexes *1*–*5*. 0.15 g of the ligand were dissolved in degassed methanol under nitrogen and the pH was adjusted to 8–9 by adding NaOH 1 M, resulting in a yellow solution. An equimolar amount of CuCl$_2$2H$_2$O in methanol was added and a dark green precipitate appeared. The suspension was stirred for 4 h at r.t. The solvent was partially evaporated under vacuum and the dark green powder was filtered off and washed with cold methanol.

[Cu(NaHL [1])Cl] **(1)**. Dark green powder. Yield: 77 %. IR (cm^{-1}): ν(OH)+ν(NH$_2$) = 3433, 3317; ν(C=N) = 1650; ν(C=S) = 1248; ν(SO$_3$) = 1170, 1040. MS-ESI (negative ions) m/z (%) = 365.2 ([CuL]$^-$, 100). Anal. Calcd. for $C_9H_9N_3NaO_5S_2CuCl$: C 25.42, H 2.13, N 9.88, S 15.08. Found: C 25.23, H 2.26, N 9.49, S 15.47. ICP calcd. for [Cu(NaHL [1])Cl]: Cu 14.94 %, Na 5.41 %. Found: Cu 15.0 ± 0.2 %, Na 5.03 ± 0.01 %.

Crystals of [Cu(HL [1])(H$_2$O)]2H$_2$O suitable for X-ray diffraction analysis were obtained by slow evaporation of a methanol solution of **(1)**.

[Cu(NaHL [2])Cl]•H$_2$O **(2)**. Dark green powder. Yield: 90 %. IR (cm^{-1}): ν(NH) = 3154, 3053; ν(C=N) = 1606; ν(C=S) = 1245; ν(SO$_3$) = 1176, 1036. MS-ESI (negative ions) m/z (%) = 393.3 ([CuL]$^-$, 100); 789.0 (([Cu(HL)]$_2$-H$^+$)$^-$, 10). Anal. Calcd. for $C_{11}H_{13}N_3NaO_5S_2CuCl \cdot H_2O$: C 28.03, H 3.21, N 8.91, S 13.61. Found: C 27.89, H 3.20, N 8.65, S 14.01. ICP calcd. for [Cu(NaHL [2])Cl]·H$_2$O: Cu 13.48 %, Na 4.88 %. Found: Cu 13.76 ± 0.03 %, Na 4.74 ± 0.01 %.

Crystals of [Cu(HL [2])(H$_2$O)$_2$]·2H$_2$O suitable for X-ray diffraction analysis were obtained by slow evaporation of a water/NaCl (0.9 %) solution of **(2)**.

[Cu(NaHL^3)Cl]•0.5H$_2$O **(3)**. Dark green powder. Yield: 91 %. IR (cm^{-1}): ν(NH$_2$) = 3364; ν(C=N) = 1605; ν(C=S) = 1251; ν(SO$_3$) = 1177, 1046. MS-ESI (negative ions) m/z (%) = 379.1 ([CuL]$^-$, 100); 415.0 ([Cu(HL)Cl]$^-$, 80). Anal. Calcd. for $C_{10}H_{11}N_3NaO_5S_2CuCl \cdot 0.5H_2O$: C 26.79, H 2.70, N 9.37, S 14.30. Found: C 26.91, H 2.89, N 9.40, S 14.29. ICP calcd. for [Cu(NaHL^3)Cl]: Cu 14.46 %, Na 5.23 %. Found: Cu 15.2 ± 0.2 %, Na 4.94 ± 0.01 %.

[Cu(HL^4)]$_2$•4H$_2$O **(4)**. Dark green powder. Yield: 77 %. IR (cm^{-1}): ν(OH)+ν(NH$_2$) = 3376, 3212; ν(NH) = 3061; ν(C=N) = 1605; ν(C=S) = 1255; ν(SO$_3$) = 1136, 1029. MS-ESI (negative ions) m/z (%) = 351.1 ([CuL]$^-$, 100); 704.1 (([Cu(HL)]$_2$-H$^+$)$^-$, 20). Anal. Calcd. for $C_8H_7N_3O_5S_2Cu \cdot 2H_2O$: C 24.71, H 2.85, N 10.81, S 16.49. Found: C 24.49, H 2.97, N 10.81, S 17.03. ICP calcd. for [Cu(HL^4)]$_2$ 4H$_2$O: Cu 16.34 %. Found: Cu 15.9 ± 0.2 %, Na 0.16 ± 0.02 %.

[Cu(HL^5)]$_2$•3H$_2$O **(5)**. Dark green powder. Yield: 68 %. IR (cm^{-1}): ν(OH) = 3310; ν(C=N) = 1598; ν(C=S) = 1243; ν(SO$_3$) = 1160, 1036. MS-ESI (negative ions) m/z (%) = 379.2 ([CuL]$^-$, 100), 760.9 (([Cu(HL)]$_2$-H$^+$)$^-$, 10). Anal. Calcd. for $C_{10}H_{11}N_3O_5S_2Cu \cdot 3H_2O$: C 27.62, H 3.94, N 9.66, S 14.74. Found: C 27.86, H 3.91, N 9.48, S 15.17. ICP calcd. for [Cu(HL^5)]$_2$ 3H$_2$O: Cu 16.61 %. Found: Cu 15.1 ± 0.3 %, Na 0.064 ± 0.003 %.

Crystals of [Cu(HL^5)(H$_2$O)]2H$_2$O suitable for X-ray diffraction analysis were obtained by slow evaporation of a solution of **5** in methanol.

[Ni(NaHL [1])Cl]•3H$_2$O **(6)**. 0.1 g of NaH$_2$L [1] were dissolved in degassed methanol under nitrogen and the pH was adjusted to 8–9 by adding NaOH 1 M, resulting in a yellow solution. An equimolar amount of NiCl$_2$6H$_2$O in methanol was added and a brownish solution was obtained. The reaction mixture was stirred for 4 h at r.t. The solvent was partially evaporated under vacuum and diethyl ether was added, obtaining the precipitation of a light brown powder, which was filtered off and washed with diethyl ether. Yield: 40 %. IR (ATR, cm^{-1}): ν(NH$_2$) = 3298; ν(NH) = 3185; ν(C=N) = 1598; ν(C=S) = 1248; ν(SO$_3$) = 1156, 1034. MS-ESI (negative ions) m/z (%) = 360.2 ([NiL]$^-$, 100), 396.0 ((Ni(HL)Cl)$^-$, 30). Anal. Calcd. for $C_9H_{10}N_3NaO_5S_2NiCl \cdot 3H_2O$: C 22.73, H 3.39, N 8.84, S 13.49. Found: C 23.07, H 3.06, N 8.66, S 13.54.

[Zn(HL [1])]$_2$•6H$_2$O **(7)**. 0.1 g of NaH$_2$L [1] were dissolved in degassed methanol under nitrogen and the pH was adjusted to 8–9 by adding NaOH 1 M, resulting in a yellow solution. An equimolar amount of Zn(CH$_3$COO) 4H$_2$O in methanol was added and the reaction mixture was stirred for 4 h at r.t. A precipitate was formed, which was filtered off and washed with diethyl ether. The crude product was recrystallized in hot water affording a light-yellow powder. Yield: 35 %. IR (ATR, cm^{-1}): ν(NH$_2$) = 3373; ν(NH) = 3181; ν(C=N) = 1636; ν(C=S) = 1251; ν(SO$_3$) = 1159, 1036. ^{1}H NMR (400 MHz, DMSO, 25 °C) δ 8.17 (s, 1H, CH=N), 6.98 (d, J = 2.2 Hz, 1H, CH$_{arom}$), 6.93 (d, J = 2.2 Hz, 1H, CH$_{arom}$), 6.13 (b, 2H, NH$_2$), 3.71 (s, 3H, OCH$_3$). MS-ESI (negative ions) m/z (%) = 366.0 ([ZnL]$^-$, 100), 735.2 (([Zn(HL)]$_2$-H$^+$)$^-$, 25). Anal. Calcd. for $C_9H_{10}N_3O_5S_2Zn \cdot 3H_2O$: C 25.51, H 3.81, N 9.92, S 15.43. Found: C 25.69, H 3.61, N 9.65, S 15.15.

Crystallography. Single crystals were mounted on a glass fiber and the intensity data were collected with a SMART APEX2 diffractometer equipped with a Bruker AXS CCD detector using Mo-Ka radiation and a graphite crystal monochromator [λ(Mo-Kα) = 0.71073 Å]. The SAINT [41] software was used for the integration of reflection intensities and scaling, and SADABS [42] for the absorption correction. The structures were solved by direct methods using SIR97 [43] and refined by full-matrix least-squares on all F2 using SHELXL97 [44] implemented in the WinGX package [45]. All the non-hydrogen atoms in the molecules were refined anisotropically. The hydrogen atoms were partly found and partly placed in ideal positions using riding models. The structures were

solved by direct methods and difference Fourier synthesis using the SHELX suite of programs as implemented within the WINGX software. Thermal ellipsoid plots were generated using the program ORTEP-333 integrated within the WinGX suite of programs.

CCDC 2347989–2347991 contain the supplementary crystallographic data of $[Cu(HL^2)(H_2O)_2]\cdot 2H_2O$, $[Cu(HL^5)(H_2O)]_2 2H_2O$, and $[Cu(HL^1)(H_2O)]_2 2H_2O$.

(http://www.ccdc.cam.ac.uk/data_request/cif).

Experiments with Human Cells. Copper complexes and free ligands, cisplatin (CDDP) and oxaliplatin (OXP) were solubilized in 0.9 % NaCl solutions. MTT (3-(4,5-dimethylthiazol-2-yl)-2,5-diphenyltetrazolium bromide), fluorogenic peptide proteasomal substrates (N-Suc-Leu-Leu-Val-Tyr-AMC, Boc-Gln-Ala-Arg-AMC, and Z-Leu-Leu-Glu-AMC; AMC = 7-amido-4-methylcoumarin), cisplatin and oxaliplatin were obtained from Sigma Chemical Co, St. Louis, USA.

Cell Cultures. Human colon (HCT-15 and LoVo) and breast (MCF-7 and MDA-MB-231) carcinoma cell lines along with non-transformed embryonic kidney (HEK293) cells were obtained from American Type Culture Collection (ATCC, Rockville, MD, USA). Human pancreatic (PSN1) carcinoma cells were obtained from European Collection of Cell Culture (ECACC, Salisbury, UK). Human ovarian 2008 cancer cells were kindly provided by Prof. G. Marverti (Dept. of Biomedical Science of Modena University, Modena, Italy). Human cervical carcinoma (A431) cells were kindly provided by Prof. F. Zunino (Division of Experimental Oncology B, Istituto Nazionale dei Tumori, Milan, Italy). The multidrug-resistant sub-line (LoVo MDR) was kindly provided by Prof. F. Majone (Dept. of Biology of Padova University, Italy). The LoVo-OXP cells were obtained as previously described [46]. Cell lines were maintained in culture in the logarithmic phase at 37 °C in a 5 % carbon dioxide atmosphere using the following media added of 10 % fetal calf serum (Euroclone, Milan, Italy), antibiotics (50 units/mL penicillin and 50 μg/mL streptomycin), and 2 mM L-glutamine: (i) RPMI-1640 medium (Euroclone) for HCT-15, PSN1,A431, MCF-7, PSN-1 and 2008 cells; (ii) F-12 HAM'S (Sigma Chemical Co.) for LoVo, LoVo MDR and LoVo-OXP cells; iii) DMEM (Sigma Chemical Co.) for MDA-MB-231 and HEK293 cells.

Spheroid Cultures. Spheroid cultures were obtained by seeding 2.5 × 10^3 HCT-15 or 2008 cells/well in round bottom non-tissue culture treated 96 well-plate (Greiner Bio-one, Kremsmünster, Austria) in phenol red free RPMI-1640 medium (Sigma Chemical Co.), containing 10 % FCS and supplemented with 20 % methyl cellulose stock solution.

MTT Assay. The growth inhibitory effect towards 2D tumor cell lines was evaluated by means of the MTT assay as previously described [47]. IC_{50} values were calculated by four parameter logistic (4-PL) model.

Acid Phosphatase (APH) Assay. An APH modified assay was used for determining cell viability in 3D spheroids, as previously described [36]. IC_{50} values were calculated with 4-PL model.

Cellular accumulation. HCT-15 cells (2.5 × 10^6) were seeded in 75 cm^2 flasks in growth medium (20 mL). After overnight incubation, the medium was replaced and the cells were treated with the tested compounds for 24 h. Cell monolayers were washed with cold PBS, harvested, and counted. The samples were treated with highly pure nitric acid (Cu: ≤0.005 μg kg^{-1}, TraceSELECT® Ultra, Sigma Chemical Co.) and transferred into a microwave teflon vessel. Afterwards, samples were mineralized by using a speed wave MWS-3 Berghof instrument (Eningen, Germany). After cooling, each mineralized sample was analyzed for copper content by means of a Varian AA Duo graphite furnace atomic absorption spectrometer (Varian, Palo Alto, CA; USA), at 324 nm. The calibration curve was obtained using known concentrations of standard solutions purchased from Sigma Chemical Co.

Reactive Oxygen Species (ROS) Production. The production of ROS was measured in HCT-15 cells (10^4 per well) grown for 24 h in a 96-well plate in RPMI medium without phenol red (Sigma Chemical Co.). Cells were then washed with PBS and loaded with 10 μM 5-(and-6)-chloromethyl-2′,7′-dichlorodihydrofluorescein diacetate acetyl ester (CM–H_2DCFDA) (Molecular Probes-Invitrogen, Eugene, OR) for 25 min, in the dark. Afterwards, cells were washed with PBS and incubated with increasing concentrations of tested compounds. Fluorescence increase was estimated utilizing the wavelengths of 485 nm (excitation) and 527 nm (emission) in an Infinite® 200 PRO (Tecan, Switzerland) plate reader. Antimycin (3 μM, Sigma Chemical Co), a potent inhibitor of Complex III in the electron transport chain, and auranofin were used as positive controls.

Mitochondrial Membrane Potential (ΔΨ). The ΔΨ was assayed using the Mito-ID® Membrane Potential Kit according to the manufacturer's instructions (Enzo Life Sciences, Farmingdale, NY). Briefly, HCT-15 cells (5 × 10^3 per well) were seeded in 96-well plates; after 24 h, cells were washed with PBS and loaded with Mito-ID Detection Reagent for 30 min at 37 °C in the dark. Afterwards, cells were incubated with increasing concentrations of tested complexes. Fluorescence intensity was estimated using a plate reader (Fluoroskan Ascent FL, Labsystems, Finland) at 490 (excitation) and 590 nm (emission). Carbonyl cyanide m-chlorophenyl hydrazone (CCCP, 4 μM), a chemical inhibitor of the oxidative phosphorylation, was used as positive control.

Quantification of thiols. HCT-15 cells (1.5 × 10^5) were seeded in a six-well plate in growth medium (4 mL). After 24 h, cells were incubated for 24 h with IC_{50} concentrations of tested compounds. Subsequently, the thiol content was measured as previously described [48].

Protein disulfide isomerase (PDI) activity. The reductase activity of PDI was assayed by measuring the PDI-catalysed reduction of insulin in the presence of increasing concentrations of the tested compounds by using PROTEOSTAT PDI assay kit (Enzo Life Sciences, Lausen, Switzerland). Experiments were performed according to the manufacturer's instructions. Briefly, copper complexes or Bacitracin (at increasing concentrations) were added to an insulin PDI solution. Subsequently, DTT was added to start PDI reduction activity and after 30 min of incubation, the reaction was stopped by adding the stop reagent mixture. The insulin precipitate was labelled with the fluorescent Proteostat PDI detection reagent and fluorescence intensity was measured at 500 nm excitation and 603 nm emission. IC_{50} values were calculated by 4-PL model.

Confocal microscopy morphological analyses. HCT-15 cells were seeded into 8-well tissue-culture slides (BD Falcon, Bedford, MA, USA) at 5 × 10^4 cells/well (0.8 cm^2). After 24 h, the cells were washed twice with PBS, and following 24 h of treatment with IC_{50} doses of the tested compound, cells were stained for 5 min with 10 μg/mL of Hoechst 33258 (20-(4-hydroxyphenyl)-5-(4-methyl-1-piperazinyl)-2,50-bi-1H-benzimidazole trihydrochloride hydrate, Sigma-Aldrich, St. Louis, MI, USA) in PBS. Samples were examined at 40 × and 10 × magnification in a Zeiss LSM 800 confocal microscope using the Zeiss ZEN 2.3 software system.

Hematoxylin-Eosin (HE) Staining. HCT-15 cells were seeded into 8-well tissue-culture slides (BD Falcon, Bedford, MA, USA) at 5 × 10^4 cells/well (0.8 cm^2). After 24 h, cells were washed twice with PBS and treated for an additional 24 h with IC_{50} concentration of tested complexes. Then, after being washed with PBS, cells were fixed in 4 % freshly prepared, ice-cold paraformaldehyde, postfixed in ethanol, and air-dried. Slides were then stained with hematoxylin and eosin before being examined at 10 × magnification in a Zeiss LSM 800 confocal microscope.

Transmission electron microscopy (TEM) analyses. About 10^6 HCT-15 cells were seeded in 24-well plates and, after 24 h incubation, were treated with IC_{50} concentrations of tested compounds and incubated for additional 24 h. Cells were then washed with cold PBS, harvested and directly fixed with 1.5 % glutaraldehyde buffer with 0.2 M sodium cacodylate, pH 7.4. After washing with buffer and postfixation with 1 % OsO_4 in 0.2 M cacodylate buffer, specimens were dehydrated and embedded in epoxy resin (Epon Araldite). Sagittal serial sections (1 μm) were counterstained with toluidine blue; thin sections (90 nm) were given contrast by staining with uranyl acetate and lead citrate. Micrographs were taken with a Hitachi H-600 electron microscope (Hitachi, Tokyo, Japan) operating at 75 kV. All photos were typeset in Corel Draw

11.

Experiments with animals. All experiments were reviewed and approved by the internal Review Board (OPBA) and authorized by the Italian Ministry of Health (authorization n. 640/2016-PR), accordingly with the current national and European regulations and guidelines for the care and use of laboratory animals (D.L. 26/2014; 86/609/EEC Directive).

***In vivo* anticancer activity toward Lewis Lung Carcinoma (LLC).** The mice were purchased from Charles River, Italy, housed in steel cages under controlled environmental conditions (constant temperature, humidity, and 12 h dark/light cycle), and alimented with commercial standard feed and tap water *ad libitum*. The LLC cell line was purchased from ECACC, United Kingdom. The LLC cell line was maintained in DMEM (Euroclone, Pero, Italy) supplemented with 10 % heat-inactivated foetal bovine serum (Euroclone, Pero, Italy), 10 mM L-glutamine, 100 U/mL penicillin, and 100 μg/mL streptomycin in a 5 % CO_2 air incubator at 37 °C. The LLC was implanted intramuscularly (i.m.) as a 2×10^6 cell inoculum into the right hind leg of 8-week-old male and female C57BL mice (24 ± 3 g body weight). After 7 days from tumor implantation (tumor visible), mice were randomly divided into 3 groups (8 animals per group) and treated with a daily i.p. injection of **5** (5 mg kg^{-1} in water), cisplatin (3 mg kg^{-1} in 0.9 % NaCl solution), or the vehicle solution (water). At day 15, animals were sacrificed, the legs were amputated at the proximal end of the femur, and the inhibition of tumor growth was determined according to the difference in weight of the tumor-bearing leg and the healthy leg of the animals expressed as a percentage referring to the control animals. Body weight measured every 2 days, starting from day 7, was taken as a parameter for systemic toxicity. Values are the means ± SD of not less than three measurements.

Statistical analysis. All values are the means ± SD of no less than three measurements starting from three different cell cultures. Multiple comparisons were made by ANOVA followed by the Tukey–Kramer multiple comparison test (*$p < 0.05$, **$p < 0.01$), using GraphPad software.

Notes

The authors declare no competing financial interest.

CRediT authorship contribution statement

Francesca Miglioli: Writing – review & editing, Data curation. **Michele De Franco:** Writing – review & editing, Data curation. **Jennifer Bartoli:** Writing – review & editing, Data curation. **Mirco Scaccaglia:** Writing – review & editing, Data curation. **Giorgio Pelosi:** Writing – original draft, Investigation, Formal analysis, Data curation. **Cristina Marzano:** Writing – review & editing, Formal analysis, Data curation. **Dominga Rogolino:** Writing – original draft, Supervision, Investigation, Data curation, Conceptualization. **Valentina Gandin:** Writing – original draft, Supervision, Funding acquisition, Data curation, Conceptualization. **Mauro Carcelli:** Writing – original draft, Supervision, Funding acquisition, Data curation, Conceptualization.

Declaration of competing interest

The authors declare that they have no known competing financial interests or personal relationships that could have appeared to influence the work reported in this paper.

Data availability

Data will be made available on request.

Acknowledgments

The authors thank “Centro Interfacoltà Misure Giuseppe Casnati” of the University of Parma for facilities. This work has benefited from the equipment and framework of the COMP-HUB Initiative, funded by the ‘Departments of Excellence’ program of the Italian Ministry for Education, University and Research (MIUR, 2018–2022 and MUR, 2023–2027). This research was also granted by University of Parma through the action “Bando di Ateneo 2023 per la ricerca”.

Appendix A. Supplementary data

Supplementary data to this article can be found online at https://doi.org/10.1016/j.ejmech.2024.116697.

References

[1] Y. Yu, D.S. Kalinowski, Z. Kovacevic, R.A. Siafakas, P.J. Jansson, C. Stefani, D. B. Lovejoy, P.S. Sharpe, P.V. Bernhardt, D.R. Richardson, Thiosemicarbazones from the old to new: iron chelators that are more than just ribonucleotide reductase inhibitors, J. Med. Chem. 52 (2009) 5271–5294, https://doi.org/10.1021/jm900552r.

[2] D.S. Kalinowski, P. Quach, D.R. Richardson, Thiosemicarbazones: the new wave in cancer treatment, Future Med. Chem. 1 (2009) 1143–1151, https://doi.org/10.4155/fmc.09.80.

[3] C.A. Kunos, E. Chu, J.H. Beumer, M. Sznol, S.P. Ivy, Phase I trial of daily triapine in combination with cisplatin chemotherapy for advanced-stage malignancies, Cancer Chemother. Pharmacol. 79 (2017) 201–207, https://doi.org/10.1007/s00280-016-3200-x.

[4] J.F. Zeidner, J.E. Karp, A.L. Blackford, B.D. Smith, I. Gojo, S.D. Gore, M.J. Levis, H. E. Carraway, J.M. Greer, S.P. Ivy, K.W. Pratz, M.A. McDevitt, A phase II trial of sequential ribonucleotide reductase inhibition in aggressive myeloproliferative neoplasms, Haematologica 99 (2014) 672–678, https://doi.org/10.3324/haematol.2013.097246.

[5] P.J. Jansson, D.S. Kalinowski, D.J.R. Lane, Z. Kovacevic, N.A. Seebacher, L. Fouani, S. Sahni, A.M. Merlot, D.R. Richardson, The renaissance of polypharmacology in the development of anti-cancer therapeutics: inhibition of the "Triad of Death" in cancer by di-2-pyridylketone thiosemicarbazones, Pharmacol. Res. 100 (2015) 255–260, https://doi.org/10.1016/j.phrs.2015.08.013.

[6] K.Y. Salim, W.R. Danter, V.S. Maleki, J. Koropatnick, COTI-2, a novel small molecule that is active against multiple human cancer cell lines in vitro and in vivo, Oncotarget 7 (2016) 41363–41379, https://doi.org/10.18632/oncotarget.9133.

[7] P. Hädinger, M.P. Müller, A. Hinz, Synthesis and reactivity of base-stabilized and base-free silaimidoyl bromides, Inorg. Chem. 63 (2024) 1997–2004, https://doi.org/10.1021/acs.inorgchem.3c03711.

[8] B.M. Zeglis, V. Divilov, J.S. Lewis, Role of metalation in the topoisomerase IIα inhibition and antiproliferation activity of a series of α-heterocyclic-N4-substituted thiosemicarbazones and their Cu(II) complexes, J. Med. Chem. 54 (2011) 2391–2398, https://doi.org/10.1021/jm101532u.

[9] V.A. Rao, S.R. Klein, K.K. Agama, E. Toyoda, N. Adachi, Y. Pommier, E.B. Shacter, The iron chelator Dp44mT causes DNA damage and selective inhibition of topoisomerase II alpha in breast cancer cells, Cancer Res. 69 (2009) 948–957, https://doi.org/10.1158/0008-5472.CAN-08-1437.

[10] A. Mrozek-Wilczkiewicz, K. Malarz, M. Rejmund, J. Polanski, R. Musiol, Anticancer activity of the thiosemicarbazones that are based on di-2-pyridine ketone and quinoline moiety, Eur. J. Med. Chem. 171 (2019) 180–194, https://doi.org/10.1016/j.ejmech.2019.03.027.

[11] V. Pósa, A. Stefanelli, J.H.B. Nunes, S. Hager, M. Mathuber, N.V. May, W. Berger, B.K. Keppler, C.R. Kowol, É.A. Enyedy, P. Heffeter, Thiosemicarbazone derivatives developed to overcome COTI-2 resistance, Cancers 14 (2022) 4455, https://doi.org/10.3390/cancers14184455.

[12] A. Popovic-Bijelic, C.R. Kowol, M.E.S. Lind, J. Luo, F. Himo, E.A. Enyedy, V. B. Arion, A. Graeslund, Ribonucleotide reductase inhibition by metal complexes of Triapine (3-aminopyridine-2-carboxaldehyde thiosemicarbazone): a combined experimental and theoretical study, J. Inorg. Biochem. 105 (2011) 1422–1431, https://doi.org/10.1016/j.jinorgbio.2011.07.003.

[13] Y. Yu, Y.S. Rahmanto, C.L. Hawkins, D.R. Richardson, The potent and novel thiosemicarbazone chelators di-2-pyridylketone-4,4-dimethyl-3-thiosemicarbazone and 2-benzoylpyridine-4,4-dimethyl-3-thiosemicarbazone affect crucial thiol systems required for ribonucleotide reductase activity, Mol. Pharmacol. 79 (2011) 921–931, https://doi.org/10.1124/mol.111.071324.

[14] P.J. Jansson, P.C. Sharpe, P.V. Bernhardt, D.R. Richardson, Novel thiosemicarbazones of the ApT and DpT series and their copper complexes: identification of pronounced redox activity and characterization of their antitumor activity, J. Med. Chem. 53 (2010) 5759–5769, https://doi.org/10.1021/jm100561b.

[15] P.V. Bernhardt, P.C. Sharpe, M. Islam, D.B. Lovejoy, D.S. Kalinowski, D. R. Richardson, Iron chelators of the dipyridylketone thiosemicarbazone class: precomplexation and transmetallation effects on anticancer activity, J. Med. Chem. 52 (2009) 407–415, https://doi.org/10.1021/jm801012z.

[16] C. Santini, M. Pellei, V. Gandin, M. Porchia, F. Tisato, C. Marzano, Advances in copper complexes as anticancer agents, Chem. Rev. 114 (2014) 815–862, https://doi.org/10.1021/cr400135x.

[17] D. Denoyer, S. Masaldan, S. La Fontaine, M.A. Cater, Targeting copper in cancer therapy: 'Copper that Cancer', Metallomics 7 (2015) 1459–1476, https://doi.org/10.1039/C5MT00149H.
[18] J. Wang, J. Li, J. Liu, K.-Y. Chan, H.-S. Lee, K.N. Lin, C.-C. Wang, T.-S. Lau, Interplay of ferroptosis and cuproptosis in cancer: dissecting metal-driven mechanisms for therapeutic potentials, Cancers 16 (2024) 512, https://doi.org/10.3390/cancers16030512.
[19] R. Ali, M. Aouida, A. Alhaj Sulaiman, S. Madhusudan, D. Ramotar, Can cisplatin therapy Be improved? Pathways that can Be targeted, Int. J. Mol. Sci. 23 (2022) 7241, https://doi.org/10.3390/ijms23137241.
[20] H. Xie, Y.J. Kang, Role of copper in angiogenesis and its medicinal implications, Curr. Med. Chem. 16 (2009) 1304–1314, https://doi.org/10.2174/092986709787846622.
[21] J.H.B. Nunes, S. Hager, M. Mathuber, V. Posa, A. Roller, E.A. Enyedy, A. Stefanelli, W. Berger, B.K. Keppler, P. Heffeter, et al., Cancer cell resistance against the clinically investigated thiosemicarbazone COTI-2 is based on formation of intracellular copper complex glutathione adducts and ABCC1-mediated efflux, J. Med. Chem. 63 (2020) 13719–13732, https://doi.org/10.1021/acs.jmedchem.0c01277.
[22] X. Wang, M. Zhu, S. Li, G. Xu, Z. Zhang, F. Yang, Novel mono-, bi-, tri- and tetranuclear copper complexes that inhibit tumor growth through apoptosis and anti-angiogenesis, J. Inorg. Biochem. 250 (2024) 112403, https://doi.org/10.1016/j.jinorgbio.2023.112403.
[23] F.N. Akladios, S.D. Andrew, C.J. Parkinson, Increased generation of intracellular reactive oxygen species initiates selective cytotoxicity against the MCF-7 cell line resultant from redox active combination therapy using copper-thiosemicarbazone complexes, J. Biol. Inorg. Chem. 21 (2016) 407–419, https://doi.org/10.1007/s00775-016-1350-2.
[24] M. Carcelli, M. Tegoni, J. Bartoli, C. Marzano, G. Pelosi, M. Salvalaio, D. Rogolino, V. Gandin, *In vitro* and *in vivo* anticancer activity of tridentate thiosemicarbazone copper complexes: unravelling an unexplored pharmacological target, Eur. J. Med. Chem. 194 (2020) 112266, https://doi.org/10.1016/j.ejmech.2020.112266.
[25] S. Hager, K. Korbula, B. Bielec, M. Grusch, C. Pirker, M. Schosserer, L. Liendl, M. Lang, J. Grillari, K. Nowikovsky, V.F.S. Pape, T. Mohr, G. Szakács, B.K. Keppler, W. Berger, C.R. Kowol, P. Heffeter, The thiosemicarbazone Me_2NNMe_2 induces paraptosis by disrupting the ER thiol redox homeostasis based on protein disulfide isomerase inhibition, Cell Death Dis. 9 (2018) 1052, https://doi.org/10.1038/s41419-018-1102-z.
[26] E. Lee, D.H. Lee, Emerging roles of protein disulfide isomerase in cancer, BMB Rep 50 (2017) 401–410, https://doi.org/10.5483/bmbrep.2017.50.8.107.
[27] S.A. Hosseini-Yazdi, A. Mirzaahmadi, A.A. Khandar, M. Mahdavi, A. Rahimian, V. Eigner, M. Dusek, G. Zarrini, Copper, nickel and zinc complexes of a new water-soluble thiosemicarbazone ligand: synthesis, characterization, stability and biological evaluation, J. Mol. Liq. 248 (2017) 658–667, https://doi.org/10.1016/j.molliq.2017.10.068.
[28] A. Sîrbu, O. Palamarciuc, M.V. Babak, J.M. Lim, K. Ohui, E.A. Enyedy, S. Shova, D. Darvasiová, P. Rapta, W.H. Ang, V.B. Arion, Copper(II) thiosemicarbazone complexes induce marked ROS accumulation and promote nrf2-mediated antioxidant response in highly resistant breast cancer cells, Dalton Trans. 46 (2017) 3833–3847, https://doi.org/10.1039/C7DT00283A.
[29] S.A. Hosseini-Yazdi, A. Mirzaahmadi, A.A. Khandar, V. Eigner, M. Dusek, M. Mahdavi, S. Soltani, F. Lotfipour, J. White, Reactions of copper(II), nickel(II), and zinc(II) acetates with a new water-soluble 4-phenylthiosemicarbazone Schiff base ligand: synthesis, characterization, unexpected cyclization, antimicrobial, antioxidant, and anticancer activities, Polyhedron 124 (2017) 156–165, https://doi.org/10.1016/j.poly.2016.12.004.
[30] E.B. Hager, B.C.E. Makhubela, G.S. Smith, Aqueous-phase hydroformylation of 1-octene using hydrophilic sulfonate salicylaldimine dendrimers, Dalton Trans. 41 (2012) 13927–13935, https://doi.org/10.1039/C2DT31471A.
[31] F. Hu, H. Hu, J. Hu, S. Zhu, J. Yang, Y. Wang, Improving selective separation of Cu (II) from acidic polymetallic media with 2-ethylhexyl 4-pyridinecarboxylate ester: extraction behaviors, coordination structure and microscopic mechanism, J. Mol. Liq. 248 (2017) 1050, https://doi.org/10.1016/j.molliq.2017.10.143.
[32] K.T. Mahmudov, M. Sutradhar, L.M.D.R.S. Martins, M.F.C.G. d. Silva, A. Ribera, A. V.M. Nunes, S.I. Gahramanova, F. Marchetti, A.J.L. Pombeiro, Mn(II) and Cu(II) complexes with arylhydrazones of active methylene compounds as effective heterogeneous catalysts for solvent- and additive-free microwave-assisted peroxidative oxidation of alcohols, RSC Adv. 5 (2015) 25979, https://doi.org/10.1039/C5RA02667A.
[33] R. Jlassi, A.P.C. Ribeiro, E.C.B.A. Alegria, H. Naili, G.A.O. Tiago, T. Ruffer, H. Lang, F.I. Zubkov, A.J.L. Pombeiro, W. Rekik, Copper(II) complexes with an arylhydrazone of methyl 2-cyanoacetate as effective catalysts in the microwave-assisted oxidation of cyclohexane, Inorg. Chim. Acta. 471 (2018) 658–663, https://doi.org/10.1016/j.ica.2017.12.001.
[34] C. Janiak, A critical account on π–π stacking in metal complexes with aromatic nitrogen-containing ligands, J. Chem. Soc. Dalton Trans. (2000) 3885–3896, https://doi.org/10.1039/B003010O.
[35] A. Podolski-Renić, A. Čipak Gašparović, A. Valente, Ó. López, J.H. Bormio Nunes, C.R. Kowol, P. Heffeter, N.R. Filipović, Schiff bases and their metal complexes to target and overcome (multidrug) resistance in cancer, Eur. J. Med. Chem. 270 (2024) 116363, https://doi.org/10.1016/j.ejmech.2024.116363.
[36] V. Gandin, C. Ceresa, G. Esposito, S. Indraccolo, M. Porchia, F. Tisato, C. Santini, M. Pellei, C. Marzano, Therapeutic potential of the phosphino Cu(I) complex (HydroCuP) in the treatment of solid tumors, Sci. Rep. 7 (2017) 13936, https://doi.org/10.1038/s41598-017-13698-1.
[37] L.A. Kunz-Schughart, J.P. Freyer, F. Hofstaedter, R.T.J. Ebner, The use of 3-D cultures for high-throughput screening: the multicellular spheroid model, J. Biomol. Screen 9 (2004) 273–285.
[38] P. Victor, D. Sarada, K.M. Ramkumar, Crosstalk between endoplasmic reticulum stress and oxidative stress: focus on protein disulfide isomerase and endoplasmic reticulum oxidase 1, Eur. J. Pharmacol. 892 (2021) 173749, https://doi.org/10.1016/j.ejphar.2020.173749.
[39] D. Tang, X. Chen, G. Kroemer, Cuproptosis: a copper-triggered modality of mitochondrial cell death, Cell Res. 32 (2022) 417–418, https://doi.org/10.1038/s41422-022-00653-7.
[40] D. Chiodi, Y. Ishihara, The role of the methoxy group in approved drugs, Eur. J. Med. Chem. (2024) 116364, https://doi.org/10.1016/j.ejmech.2024.116364.
[41] SAINT: SAX, Area Detector Integration, Siemens Analytical Instruments Inc., Madison, Wisconsin, USA.
[42] G. Sheldrick, SADABS: Siemens Area Detector Absorption Correction Software, University of Goettingen, Germany, 1996.
[43] A. Altomare, C. Burla, M. Camalli, G.L. Cascarano, C. Giacovazzo, A. Guagliardi, A. G.G. Moliterni, G. Polidori, R. Spagna, J. Appl. Crystallogr. 32 (1999) 115–119.
[44] G.M. Sheldrick, A short history of SHELX, Acta Crystallogr. A64 (2008) 112–122, https://doi.org/10.1107/S0108767307043930.
[45] L.J. Farrugia, WinGX suite for small-molecule single-crystal crystallography, J. Appl. Crystallogr. 32 (1999) 837–838, https://doi.org/10.1107/S0021889899006020.
[46] V. Gandin, M. Pellei, F. Tisato, M. Porchia, C. Santini, C. Marzano, A novel copper complex induces paraptosis in colon cancer cells via the activation of ER stress signalling, J. Cell Mol. Med. 16 (2012) 142–151, https://doi.org/10.1111/j.1582-4934.2011.01292.x.
[47] M.C. Alley, D.A. Scudiero, A. Monks, M.L. Hursey, M.J. Czerwinski, D.L. Fine, B. J. Abbott, J.G. Mayo, R.H. Shoemaker, M.R. Boyd, Feasibility of drug screening with panels of human tumor cell lines using a microculture tetrazolium assay, Cancer Res. 48 (1988) 589–601.
[48] M.P. Rigobello, V. Gandin, A. Folda, A.-K. Rundloef, A.P. Fernandes, A. Bindoli, C. Marzano, M. Bjoernstedt, Treatment of human cancer cells with selenite or tellurite in combination with auranofin enhances cell death due to redox shift, Free Radic. Biol. Med. 47 (2009) 710–721, https://doi.org/10.1016/j.freeradbiomed.2009.05.027.